ACS Catalysis

RESEARCH ARTICLE

pubs.acs.org/acscatalysis

Au/Y-TiO_2 Catalyst: High Activity and Long-Term Stability in CO Oxidation

Rodolfo Zanella,*[,†] Vicente Rodríguez-González,[‡] Yamin Arzola,[†] and Albino Moreno-Rodriguez[§]

[†]Centro de Ciencias Aplicadas y Desarrollo Tecnológico, Universidad Nacional Autónoma de México, Circuito Exterior S/N, Ciudad Universitaria, A. P. 70-186, Delegación Coyoacán, C.P. 04510, México D. F., Mexico

[‡]División de Materiales Avanzados, IPICYT, Instituto Potosino de Investigación Científica y Tecnológica, Camino a la Presa San José 2055 Col. Lomas 4a. sección C.P. 78216, San Luis Potosí, S.L.P., Mexico

[§]Departamento de Química General, Facultad de Ciencias Químicas, Benemérita Universidad Autónoma de Puebla, 14 Sur 6301, Puebla, Puebla 72570, Mexico

ABSTRACT:

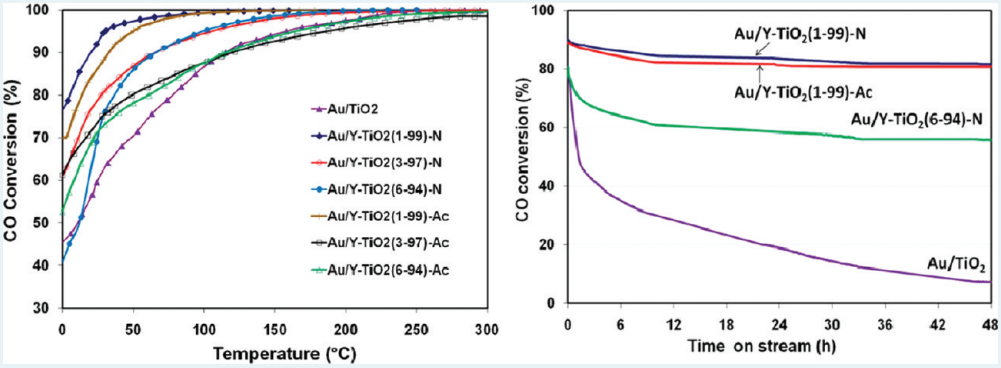

Gold catalysts supported on TiO_2 doped with Y (1, 3, and 6 wt % of Y) were prepared by the deposition-precipitation with urea method. Two yttrium precursors were used: yttrium acetylacetonate and yttrium nitrate. The Y-TiO_2 supports prepared by the sol−gel method allowed the formation of solids with high specific surface area. The incorporation of yttrium restricted the growth of TiO_2 anatase crystals and hindered the transformation to the rutile phase. The average gold particle size was very similar in all the prepared catalysts (~3 nm). Au/Y-TiO_2 catalysts showed higher activity and stability at room temperature than Au/TiO_2 in the CO oxidation reaction. This behavior is related to the strong anchoring of the gold particles on the structural defects and oxygen vacancies of the support caused by the doping of the anatase with yttrium. The variation of the yttrium precursor (acetylacetonate or nitrate) did not have an important effect on the catalytic activity or the temporal stability of the catalysts. In the samples with a high content of Y, High Resolution Transmission Electron Microscopy (HRTEM) results suggest the segregation of yttrium as Y_2O_3 on the surface of TiO_2. The presence of Y_2O_3 crystals on the TiO_2 surface had a detrimental effect on the catalytic activity.

KEYWORDS: gold, titania, yttrium doped titania, CO oxidation, stabilization of gold catalysts

1. INTRODUCTION

Since the discovery in the late 1980s that gold is catalytically active when it is dispersed as small particles on an oxide support, the preparation of gold-based catalysts has been widely studied.[1−5] They are active in many reactions of both industrial and environmental importance. The most remarkable catalytic properties of supported gold have been obtained for the reaction of CO oxidation at ambient temperature.[3−6] The catalytic activity strongly depends on the dimensions of the gold particles and is the highest in the range of 1−3 nm,[7−12] the material used as support, the synthesis method, and the catalyst activation procedure.[7,10,13,14]

The dimensions of gold particles in Au catalysts depend on the preparation method,[15] the parameters of the preparation (contact time, pH, T), the parameters of thermal treatment used to reduce Au^{III} into Au^0,[8,16,17] and also depend on the interaction between these particles and the support.[8,18]

If this interaction is weak, during the catalytic reaction, the gold particles move on the surface of the support through Ostwald ripening, producing larger gold particles and losing their catalytic activity for the oxidation of CO.[19−21] The catalytic activity of gold catalysts for the oxidation of CO is also decreased by the formation of carbonates adsorbed on the reactive sites of the catalysts.[18,22,23] The deactivation produced in this way is reversible, and after heating the catalyst, the activity concerning the formation of CO_2 is restored.[18,24] On the other hand,

Received: June 22, 2011
Revised: November 10, 2011
Published: November 14, 2011

the agglomeration of the small Au particles giving larger but less active particles[19,20,25,26] produces an irreversible and more important deactivation.

Hence, in spite of their good initial catalytic activity, supported Au catalysts have still very few commercial applications.[27] Thus, it is important to stabilize the gold nanoparticles in the 1−3 nm size range. In this way, the support plays a major role for the stability of the gold particles that depends on both its structure and the specific interaction occurring between the gold particles and the support.

A way to overcome the deactivation process is to produce oxygen vacancies on the surface of the support particles.[28−30] These oxygen vacancies generate crystalline defects that work as pinning centers for the gold particles. The steps on the surface of the support particles are also crystalline defects that could work as pinning centers for the gold particles.[31] Theoretical calculations have demonstrated that the gold particles bind stronger to a defect-rich surface than to a defect-deficient surface and that a significant charge transfer occurs from the titania support to the Au particles,[32−35] which could explain the catalytic activity of the Au particles for the oxidation of CO.

Many studies have been done to stabilize the supported gold nanoparticles. It has been suggested that the use of binary mixed oxides as gold supports could be a good solution for the stabilization of gold nanoparticles.[36] The gold particles can be anchored to the support, which stabilizes them and prevents their sintering.[37−46] For example, Yan et al.,[46] prepared a highly stable catalyst by impregnation of gold over an alumina thin layer on TiO_2 (anatase) (Al_2O_3/TiO_2), the catalysts showed high activity for the CO oxidation even after calcination of the catalyst at 773 K. The high resolution transmission electron microscopy (HRTEM) observations showed that the size of the Au particles increases markedly at high temperatures on TiO_2 but slightly on Al_2O_3/TiO_2.[46] On the other hand, Venezia et al.[45] and Tai et al.[44] reported similar findings using TiO_2/SiO_2 mixed oxides as gold supports. It has been also reported that addition of iron to TiO_2, SnO_2, or CeO_2 diminishes the deactivation rate.[47] Goodman et al.,[48] reported the stabilization of highly active Au nanoparticles by surface defects via the substitution of Si with Ti in a silica thin film. Some of us reported that Au/In-TiO_2 catalysts showed higher activity and stability at room temperature than Au/TiO_2.[49] This behavior was related to the strong anchoring of the gold particles on the structural defects of the support caused by the doping of the anatase support with indium. Moreover, very recently a study about the incorporation of yttrium in TiO_2 for the preparation of gold catalysts was reported.[50] It was shown that the incorporation of yttrium in TiO_2 lattice favors the formation of oxygen vacancies, which are the preferred adsorption sites for Au nanoparticles, acting as nucleation centers for Au atoms. The Au particle size obtained in that work, using the deposition precipitation (DP) with NaOH method was rather large (9−11 nm); however, it was shown that the incorporation of yttrium increased the activity for CO oxidation.[50]

The goal of this work was to prepare Au/TiO_2 and Au/Y-TiO_2 catalysts to study their catalytic performance and stability as a function of time in the CO oxidation reaction. The Y-TiO_2 supports were prepared by the sol−gel method and the Au supported nanoparticles were obtained from the DP−Urea process. The catalysts were characterized by X-ray diffraction, nitrogen physical adsorption (BET method), photoluminescence (PL), UV−visible, FTIR, and Raman spectroscopy, H_2-TPR, HRTEM, and high-angle annular dark-field scanning transmission electron microscopy (HAADF). The catalytic activity and stability of the catalysts in the CO oxidation was performed using a reactor coupled to a GC analytical apparatus.

2. EXPERIMENTAL SECTION

2.1. Catalyst Preparation. *2.1.1. Preparation of the Y-TiO_2 Supports.* The sol−gel mixed oxides were prepared by using titanium(IV) butoxide (Aldrich, 98%) and yttrium(III) acetylacetonate hydrate (Aldrich, 99.95%) or yttrium(III) nitrate hexahydrate (Aldrich, 99.8%) as initial precursors; 21.5 mL of titanium butoxide was added dropwise to a vessel containing a basic homogeneous solution (pH = 9) containing 6 mL of distilled water, 16.6 mL of NH_4OH (Aldrich, 28.0−30.0% as NH_3), 150 mL of *n*-butanol (ACS, 99.4%), 1 g of polyvinylpyrrolidone (PVP-29, Aldrich >98%), and the corresponding amount of yttrium precursor calculated to provide 1, 3, and 6 wt % of Y in the final Y-TiO_2 sample. Afterward, the solution was maintained under reflux at 70 °C for 4 h until gelling. Then, the solution obtained was submerged in a cold bain-marie (T = 3 °C) for 15 min. Then the solid was slowly dried in air at 70 °C for 12 h and calcined in air at 500 °C for 4 h by using a programmed heating rate of 2 °C/min. The obtained supports were labeled as Y-TiO_2(1-99), Y-TiO_2(3-97), and Y-TiO_2(6-94) respectively, followed by N or Ac for the case in which yttrium nitrate or yttrium acetylacetonate was used as yttrium precursor.

2.1.2. Preparation of the Catalysts. The catalysts were prepared in the absence of light, since it is known that light decomposes and reduces the gold precursors. The preparation of the gold nanoparticles was performed by deposition-precipitation with urea (DP Urea).[15,51] The gold precursor, $HAuCl_4$ (4.2×10^{-3} M) and the urea (0.42 M) were dissolved in 20 mL of distilled water; the initial pH of the solution was 2.4. Then, one gram of the titania or titania-yttrium supports was added to this solution under constant stirring; thereafter, the suspension temperature was increased to 80 °C and kept constant for 16 h. The urea decomposition led to a gradual rise in pH from 2.4 to 7.[15] The amount of gold in the solution corresponded to a maximum gold loading of 3 wt % on the supported catalyst.

After the deposition-precipitation procedure, all the samples were centrifuged, washed with water at 50 °C and then centrifuged four times and dried under vacuum for 2 h at 100 °C. The thermal treatments were performed in a U reactor with a fritted plate of 1.5 cm of diameter; the calcination under a flow of dry air ($1\ mL\ min^{-1}\ mg_{sample}{}^{-1}$) was performed at 300 °C, for 2 h. All the samples were stored at room temperature under vacuum in a desiccator away from light to prevent any alteration.[16]

2.2. Characterization. The physical adsorption of N_2 at −196 °C was done using a Quantachrome Autosorb 1 automatic instrument on samples previously outgassed at 150 °C. The Brunauer−Emmett−Teller method (BET method) was applied to calculate the specific surface area. The X-ray diffraction (XRD) powder patterns of the calcined samples were recorded on a Bruker D8 Advance diffractometer by using CuKα radiation (within the 2θ range going from 10° to 70°). The titania average crystallite size was calculated by the Scherrer equation.

The chemical analysis of Au and Y in the samples to determine the actual loading was performed by energy dispersive X-ray spectroscopy (EDS) using an Oxford-ISIS detector coupled to a scanning electron microscope (JEOL JSM-5900-LV). In every sample more than 30 different areas were analyzed, and the average metal concentration for every sample is reported.

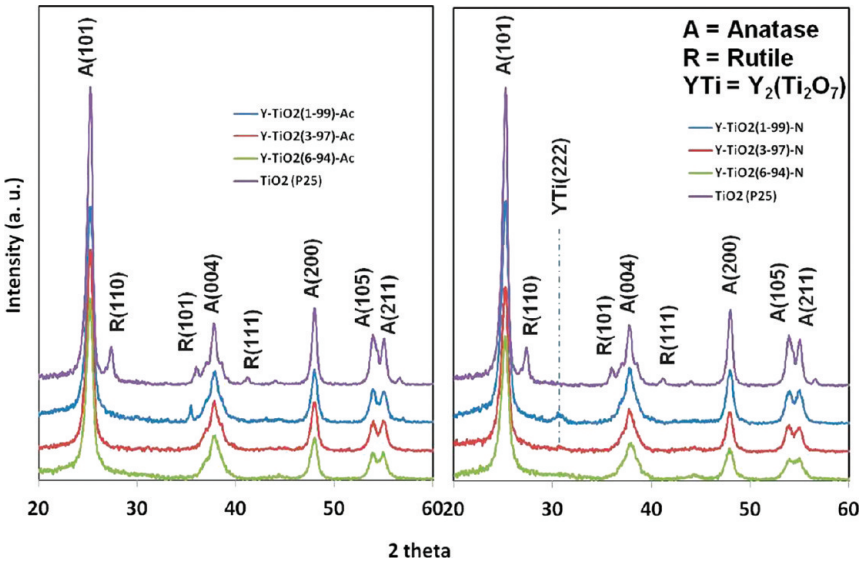

Figure 1. X-ray diffraction patterns of the studied Y-TiO_2 samples. For comparison the profile of TiO_2 Degussa P25 is shown.

The chemical analysis was performed after the thermal treatment of the samples. The Au and Y loadings are expressed as g/g sample. Some of the samples were also analyzed by Inductively Coupled Plasma (ICP) in a Perkin-Elmer, Optical Emission Spectrometer Optima 4300 DV. The measured concentration values in both techniques were similar and differed in less than 10%.

The PL excitation and emission spectra were recorded at room temperature on a Perkin-Elmer LS 55 spectrofluorometer with a quartz solid sample holder. The lamp intensity correction is performed automatically by this instrument that measures the excitation light intensity with an additional photomultiplier tube and performs the correction accordingly before displaying the data. The emission spectra were collected using a conventional setup at an excitation wavelength of 330 nm. Experimental precautions were taken for getting comparable intensities: the same sample preparation procedure, parameters, and alignment in the device were used.

The infrared spectroscopy experiments were carried out using a Nicolet Nexus 670 spectrophotometer. In each experiment, about 0.005 g of the catalysts were mixed with 0.1 g of KBr previously dried. The mixture was pressed in a pellet and analyzed in IR transmission mode. The spectra were collected under air at room temperature from 128 scans with a resolution of 4 cm^{-1}.

Diffuse reflectance UV−visible spectra of the catalysts were obtained using an Ocean Optics USB2000 miniature fiber optic spectrometer. The equipment was calibrated with a Spectralon standard (Labsphere SRS-99-010, 99% reflectance) then, the Eg was estimated from the plot of the absorbance vs wavelength of the absorbed light for indirect allowed transitions. The Raman spectra were recorded on a Renishaw MicroRaman Invia Spectrometer, equipped with an argon laser source. The laser excitation line was 514 nm, and the power was of 25 mW.

Hydrogen temperature programmed reduction (H_2-TPR) of the dried catalysts (100 mg) was performed in a RIG-150 unit under a flow of 10% H_2/Ar gas mixture (30 $mLmin^{-1}$) and a heating rate of 10 °C/min from room temperature to 600 °C. H_2O produced during the reduction process was trapped before the TCD detector. Bulk CuO was used as a reference for the calibration of the TCD signal.

HRTEM observations of the calcined catalysts were performed in a JEM 2010 FasTem analytical microscope equipped with a Z-contrast annular detector that allows obtaining high-angle annular dark-field scanning (HAADF) images. The average size of the gold particles and the histograms of the particle sizes were established from the measurement of 800 to 1000 particles obtained by HAADF observations. The size limit for the detection of gold particles on TiO_2 was about 0.5 nm. The average particle diameter d_s was calculated using the following formula: $d_s = \Sigma n_i d_i / \Sigma n_i$ where n_i is the number of particles of diameter d_i.

2.3. Catalytic Activity Measurements. The CO oxidation reaction was studied in a flow reactor at atmospheric pressure and increasing temperature range from 0 to 300 °C (light off test). A 0.04 g portion of dried catalyst was first activated in situ in a flow of 40 mL/min of air with a heating rate of 2 °C/min up to the final activation temperatures followed by a temperature plateau of 2 h. After this treatment, the sample was cooled to 0 °C under the same gas. The reactant gas mixture (1% vol. CO and 1% vol. O_2 balanced N_2) was introduced with a total flow rate of 100 mL/min, and the heating rate was 2 °C/min. The gases were analyzed with an online gas chromatograph Agilent Technologies 6890N equipped with a FID detector, a methanizer, and an HP Plot Q column.

Stability of the catalysts versus time on stream was examined at 15 °C during a 48 h run after activation in situ and under the same conditions as described above.

3. RESULTS AND DISCUSSION

3.1. Supports Characterization. The XRD patterns of Y-TiO_2 supports with different Y loadings show the formation of anatase as the main crystalline TiO_2 phase (JCPDF 78-2486) (Figure 1). In the samples yttrium oxide crystals are not observed in any of the Y-TiO_2 samples by this technique, indicating even that yttrium effectively doped TiO_2 or the formation of yttrium oxide with nanometric size, which is not detectable by XRD. It is important to consider that the low contents of yttrium make its

dx.doi.org/10.1021/cs200332v |ACS Catal. 2012, 2, 1–11

detection difficult because in some samples it is under the detection limit of the technique. The peak corresponding to the (101) reflection of anatase (25.418 of 2θ; JCPDF 78-2486) is slightly broad for the sample with the highest yttrium content of 6%. It seems that the incorporation of yttrium restricts the transformation of the TiO_2 anatase phase to the rutile TiO_2 crystalline phase. Normally, the rutile phase starts to grow at 450 °C in sol−gel materials.[52] It means that yttrium doping favors the retention of the anatase phase on these sol−gel materials. Moreover, in the Y-TiO_2 samples with the lowest Y content (1%) low intensity peaks were detected that can be related to the oxygen deficient titanium oxide structure Ti_5O_9 (JCPDF 71-0627). In addition, in samples Y-TiO_2 (1-99)-N and Y-TiO_2 (3-97)-N, a diffraction line at about 30.5° is observed. This diffraction line is not present in the sample obtained using yttrium acetylacetonate as precursor. According to the XRD pattern from the ICSD database, this line can be assigned to defective titanium oxide structures (Ti_5O_9 or $Ti_{10}O_{18}$) but also to a disordered pyrochlore ($Y_2Ti_2O_7$) structure. The complexity of the titanium oxide structures and the sol−gel synthesis could have favored the production of both types of structures.

The Raman spectra are shown in Figure 2. The nanocrystalline powders show characteristic active modes at 144, 200, 402, 502, 522, and 642 cm^{-1} which are attributed to the E_g, B_{1g}, A_{1g}, B_{2g}, and E_g vibrational modes of TiO_2, respectively.[53] These active modes indicate the presence of the anatase phase.[53] Comparing to the TiO_2 bare materials, a slight Raman shift is observed in the E_g mode peaks that could support the assumption that some Y^{3+} cations are inserted in the titania framework.[54] The Y^{3+} radius is 104 pm (hexacoordinated), which compared with the Ti^{4+} radius of 74.5 pm (hexacoordinated) is too high to expect a large substitution.[55] The difficulty in having long extent substitution is obvious because of the big difference in the atomic radius of Ti^{4+} and Y^{3+}. It must be noted that the observed shift is also feasible because of the effect of decreasing crystallite size in the Y-doped TiO_2 nanoparticles. Once the crystallite size decreases a few nanometers, the effects on the vibrational properties of these materials might occur. Also, the formation of some oxygen deficient titanium oxide structure Ti_5O_9 and pyrochlore structures ($Y_2Ti_2O_7$) may possibly contribute to the shift observed in the Raman spectra. The full width at half-maximum (fwhm) of the 144 cm^{-1} Raman peak was obtained using a MicroCal OriginPro 8SR1. The values are listed in Table 1. The fwhm varies from 10.6 to 12.6 cm^{-1}. The Raman shift of Y-TiO_2 samples is related to the stress/strain state. The width of the Raman peak is related to the quality of the crystal (deformation, thickness, and defects). According with the values of fwhm it could be proposed that Y-TiO_2 materials doped with yttrium nitrate have more crystalline defects than Y-TiO_2 materials doped with yttrium actilacetonate.

Y-TiO_2 and parent anatase TiO_2 were analyzed by PL using an excitation wavelength of 330 nm. PL characterization is an effective way to investigate the electronic structure and the optical characteristics of semiconductor nanomaterials by which information such as the surface oxygen vacancies and the defects can be obtained.[56−59] The results obtained for Y-TiO_2-N samples are presented in Figure 3; similar results were obtained for Y-TiO_2-Ac series. As can be observed in Figure 3, well-defined

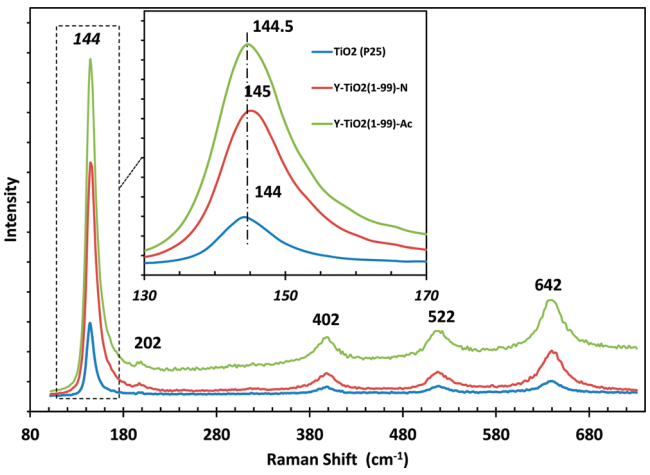

Figure 2. Raman spectra of TiO_2, Y-TiO_2 (1-99)-N and Y-TiO_2 (1-99)-Ac supports.

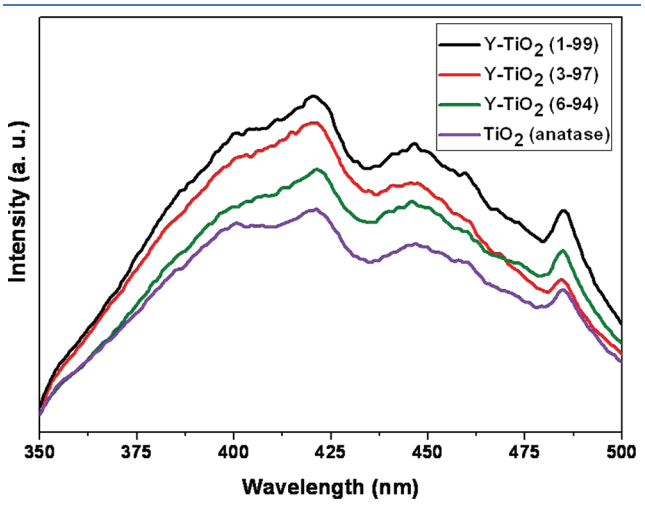

Figure 3. PL spectra of the Y-TiO_2-N samples. Parent TiO_2 is shown for comparison.

Table 1. Characteristics of the Studied Oxides

sample	Y precursor	theoretical Y loading, wt %	actual Y loading, wt %	BET surface area (m^2/g)	crystallite size (nm)	Eg (eV)	fwhm[a] (cm^{-1})
Y-TiO_2(1-99)-N	$Y(NO_3)_3$	1	0.54	73	11.8	3.18	12.6
Y-TiO_2(3-97)-N	$Y(NO_3)_3$	3	2.1	98	11.0	3.18	12.4
Y-TiO_2(6-94)-N	$Y(NO_3)_3$	6	5.6	112	10.3	3.19	12.2
Y-TiO_2(1-99)-Ac	$Y(CH_3COCH{=}COCH_3)_3$	1	0.52	64	13.9	3.16	11.9
Y-TiO_2(3-97)-Ac	$Y(CH_3COCH{=}COCH_3)_3$	3	2	78	11.6	3.16	11.6
Y-TiO_2(6-94)-Ac	$Y(CH_3COCH{=}COCH_3)_3$	6	5.1	98	11.0	3.19	10.6
TiO_2 (P25)				53	19.91	3.20	9.4

[a] Full Width at Half-Maximum calculated from Raman spectra.

dx.doi.org/10.1021/cs200332v |ACS Catal. 2012, 2, 1−11

peaks at 398, 423, 446, 462, and 485 nm are observed. The peak at 398 nm can be assigned to self-trapped excitation localized in the TiO_6 octahedron, and the peak at 446 nm to surface defects.[59−65] Serpone et al. propose that the spectral band centered near 420 nm[66] involves color centers associated with oxygen vacancies created during the doping of TiO_2. The peaks at 462 and 486 nm have been also attributed to oxygen vacancies.[59−65,67] It is well-known that a higher number of surface defects and oxygen vacancies result in higher PL intensity.[59] As can be observed in Figure 3, the Y-TiO_2 samples present higher intensity than parent TiO_2 indicating that oxygen vacancies and other defect sites were created in the doped samples. Especially, the Y-TiO_2 (1-99) sample has the highest intensity, indicating that this sample has the highest quantity of surface defects and oxygen vacancies.

The specific surface area for the different Y-TiO_2 samples is reported in Table 1. High specific surface areas (64−112 m^2/g) for all the solids were obtained. The highest BET surface area is observed with the Y-TiO_2 (6-94)-N (112 m^2/g) sample. In both cases (nitrate or acetylacetonate precursor), the BET surface area increases with the Y content in the sample. To understand the increase of surface area, the crystallite sizes were calculated from the peak width using the Scherrer equation: $D = k\lambda/\beta \cos \theta$, where D is the crystallite size, k is a constant (in this study k = 0.89), λ is the CuK X-ray wavelength (1.5406 Å), and β is the half-width of the peak at 2θ. The results are shown in Table 1, at higher content of yttrium, that is, Y-TiO_2 (6-94) samples, the smaller crystallite size is obtained (∼10 nm) with both precursors, which reveals that doping TiO_2 with yttrium cations can slightly prevent the growth of the crystallite size; smaller crystallite size could lead to enhanced surface area on modified TiO_2 supports. It must be noted that in addition to the decrease of the crystallite size as the theoretical Y loading increased from 1 to 6% in the sample, the average porous diameter slightly decreased from 34 to 31 Å as the Y loading increased in both series of samples. Analogous crystallite size was reported when TiO_2 was doped with indium; the crystallite size was also diminished from 24 nm (undoped) to 9 nm (12 wt %) by increasing the content of indium.[49]

TEM and HRTEM observations of the oxides were carried out to try to detect yttrium particles and titanium oxide microstrains at the atomic scale. Figure 4 shows selected images of Y-TiO_2 (6-94) samples synthesized with a nitrate or acetylacetonate precursor. The overview image of yttrium TiO_2 doped semiconductors exhibited similar morphological features, whereas on the border of TiO_2 modified particles, thin TiO_2 sheet-like structures are observed. In particular, in the sheet-like structures two different interplanar distances were measured by FFT on the image, 0.35 nm corresponding to the anatase (101) TiO_2 phase, and a lattice fringe of about 0.27 nm that can be correlated with the lattice constant for yttrium ($11\bar{2}$), 0.271 nm, according to the JCPDS standard PDF # 47-1274. These HRTEM results suggest the segregation of yttrium as Y_2O_3 on the surface of TiO_2 in the samples with a high content of Y. In the samples with low content of Y (Y-TiO_2(1-99)), no Y_2O_3 crystal was detected.

According to the characterization of the supports, it can be proposed that at low yttrium loadings (<1 wt % Y), yttrium is mainly doping TiO_2; when the Y loading is increased, that is, Y-TiO_2 (3-97) and Y-TiO_2 (6-94) samples, some yttrium oxide nanoparticles are highly dispersed on the anatase surface. Doping titania with a trivalent cation like Y^{3+} naturally gives rise to structures with oxygen vacancies; when the Y atoms enter into substitutional sites at the TiO_2 surface, the local geometry must strongly relax to accommodate the Y atom.[50] It has been shown by DFT calculations that on an Y-TiO_2 (anatase) system, only a limited amount of surface Ti atoms can be substituted by yttrium.[50] That explains the fact that only very low Y loadings can be introduced to the TiO_2 structure; for high Y loadings (3 or 6 wt %), the excess of yttrium is displaced to the TiO_2 surface, forming small Y_2O_3 crystals. In the doped Y-TiO_2 systems, the oxygen vacancies generated to balance the charge (bridge surface oxygen atoms) were found to be preferential adsorption sites for Au atoms to form nanoparticles, acting as nucleation centers that favor the dispersion of the catalyst active phase over the support surface.[50]

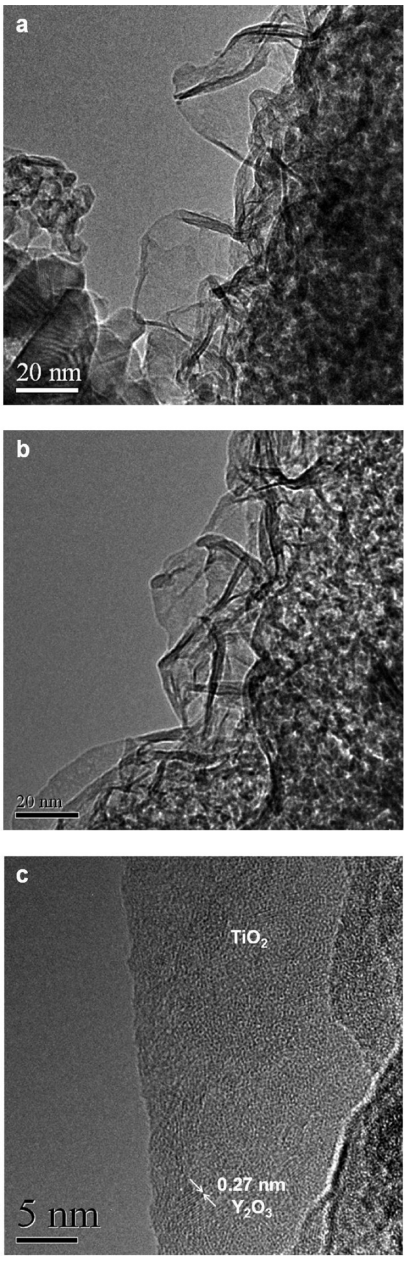

Figure 4. TEM images of (a) Y-TiO_2 (6-94)-N, (b) Y-TiO_2 (6-94)-Ac supports showing thin TiO_2 sheet-like structures, (c) HRTEM image of the sample Y-TiO_2 (6-94)-N showing an individual Y_2O_3 crystal supported on a thin TiO_2 sheet-like structure.

Table 2. Actual Au Loading, Average Gold Particle Size, and Experimental H/Au Ratio of the Studied Catalysts Activated in Air at 300 °C

catalyst support	actual Au loading, wt %[a]	average Au particle size (nm)	standard deviation (nm)	experimental H/Au ratio[b]
Y-TiO_2 (1-99)-N	2.6	3.0	0.85	1.39
Y-TiO_2 (3-97)-N	2.7	2.9	0.88	1.37
Y-TiO_2 (6-94)-N	2.4	3.1	0.94	1.33
Y-TiO_2 (1-99)-Ac	2.5	2.8	0.90	1.61
Y-TiO_2 (3-97)-Ac	3.0	3.3	0.95	1.50
Y-TiO_2 (6-94)-Ac	2.8	3.1	0.85	1.71
TiO_2 (P25)	2.9	3.1	0.86	1.48

[a] The theoretical gold loading was in all cases 3 wt %. [b] Calculated from TPR results.

3.2. Catalysts Characterization. Table 2 shows the actual gold loadings in wt % for the prepared catalysts. As expected, in all cases, more than 80% of the gold present in solution (equivalent to 3 wt %) was deposited on the support. Related to yttrium loadings, about 60% of the yttrium present in the precursor was incorporated to TiO_2 in Y-TiO_2 (1-99); for Y-TiO_2 (3-97) and Y-TiO_2 (6-94) samples about 67% and 85% of yttrium was respectively incorporated. As shown by HRTEM (Figure 4), in these last samples, a mixed oxide Y_2O_3−TiO_2 was formed. Similar results were reported by Plata et al.[50] who observed the presence of nonstoichiometric pyrochlore crystals when TiO_2 was doped with 20 wt % of Y.

Figure 5 shows the high-angle annular dark-field scanning transmission electron microscopy (HAADF-STEM) images of the gold nanoparticles supported on doped Y-TiO_2-N mixed oxides. As it can be seen in Figure 5, gold nanoparticles are well dispersed on the support, when Y is added to TiO_2, the average size of the gold particles does not change significantly in comparison with the Au/TiO_2 reference catalysts. In all cases, including the Au/TiO_2 catalysts, the average gold particle size was about 3 nm (Table 2). Moreover, no gold peaks are observed by XRD analysis of the catalysts. As it is well-known, highly dispersed gold nanoparticles smaller than 5 nm cannot be detected by XRD; this is in good agreement with the HAADF results (Figure 5).

Figure 6 shows HRTEM images of gold nanoparticles supported on Y-TiO_2 samples. The HRTEM image of the Au/Y-TiO_2(1-99) catalyst (Figure 6a) shows some anatase crystals showing the (101) crystallographic plane with small gold particles deposited on it. As shown above, in the samples with the higher Y loading (3 and 6 wt %), individual Y_2O_3 crystals were detected on the surface of TiO_2 crystals by HRTEM (Figure 4); Figures 6b and 6c correspond to catalysts with a theoretical Y loading of 6%. In Figure 6b, not well crystallized gold nanoparticles are deposited on an Y_2O_3 or $Y_2Ti_2O_7$ crystallite, and a gold nanoparticle is also deposited on an anatase crystallite. In Figure 6c a gold nanoparticle (Au^0 (111) JCPDS 4-784) is observed on the edge of an Y_2O_3 crystallite (112) JCPDS 47-1274. These images also reveal the presence of a large number of defects on the surface of the catalyst support, which could work as particle pinning centers for the gold particles.

The reducibility of the catalysts was studied by TPR. Figure 7 displays the TPR profiles of Au/TiO_2 and the Au/Y-TiO_2 samples. In the case of Au/TiO_2, the reduction profile is characterized by a peak with a maximum at T = 130 °C. The reduction of the sample begins at 100 °C and ends at ≈155 °C. A low temperature reduction peak like this has already been observed for Au/TiO_2 samples,[68−70] and assigned to the reduction of Au^{3+} or Au^+ ions to metallic gold nanoparticles. For the Au/Y-TiO_2-N and Au/Y-TiO_2-Ac samples, the reduction profile is characterized by a peak with a maximum at temperatures between 121 °C (for (1-99) samples) and 112 °C (for (6-99) samples), that is, the maximum of the peak is systematically displaced to lower temperatures as the Y loading was increased in the support. The temperature of the end of the reduction was also slightly displaced to lower temperatures as the Y loading was increased. The displacement of the maximum of the peak of reduction to lower temperatures as the Y loading is increased could be related with the presence of small crystals of Y_2O_3 on the surface of TiO_2 or with the increase of the number of surface defects on TiO_2. It has been previously shown that defective structures caused by the dopants with an oxidation state lower than (+4) introduced in oxides create vacancies which leads to higher lattice oxygen mobility resulting in enhanced reduction processes.[71] It is important to note that as Y_2O_3 is a nonreducible oxide, no peaks associated to the reduction of Y_2O_3 were observed in the TPR profiles.

Quantitative measurements of the H_2 consumption during the TPR experiments, characterized by the experimental H/Au ratio (Table 2), showed for Au/TiO_2 and Au/Y-TiO_2 samples values in the range 1.3−1.7 which is close to the stoichiometric value expected for the Au^{3+} reduction process taking into account the actual gold loading as determined by EDS analysis. In the case of Au/Y-TiO_2(1-99)-Ac, Au/Y-TiO_2(6-94)-Ac catalyst (Table 2), an enhanced reduction at low-temperatures is observed as confirmed by the slightly higher values of the experimental H/Au ratio compared to the stoichiometric value. This result could indicate both the reduction of Au^{3+} species and a slight reduction of surface titania species or the reduction of remaining species of the Y precursor.

TheY-TiO_2 samples and the Au/Y-TiO_2 catalysts were studied by UV−visible spectroscopy. The band gap energies (Eg) of the Y-TiO_2 samples are in the range from 3.16 to 3.19 eV (Table 1). The effect of yttrium present in the composite on the semiconductor properties is negligible. Practically, the band gap energy is not modified by the incorporation of Y. As reported by Serpone,[66] in our case the band gap energy practically was not shifted to the visible region compared with bare TiO_2. Thus, the Y^{3+}-doping implicates defects associated with oxygen vacancies where gold atoms were preferentially deposited. Hence, color centers that can be attributed to the formation of distinct atomic defects including oxygen vacancies were formed in the doped TiO_2 which may have worked as pinning centers for gold nanoparticles.

When gold nanoparticles were deposited on the supports, an additional absorption band with a maximum centered at 550 nm was observed. This band is characteristic of the surface plasmon resonance of gold nanoparticles and is directly related with the

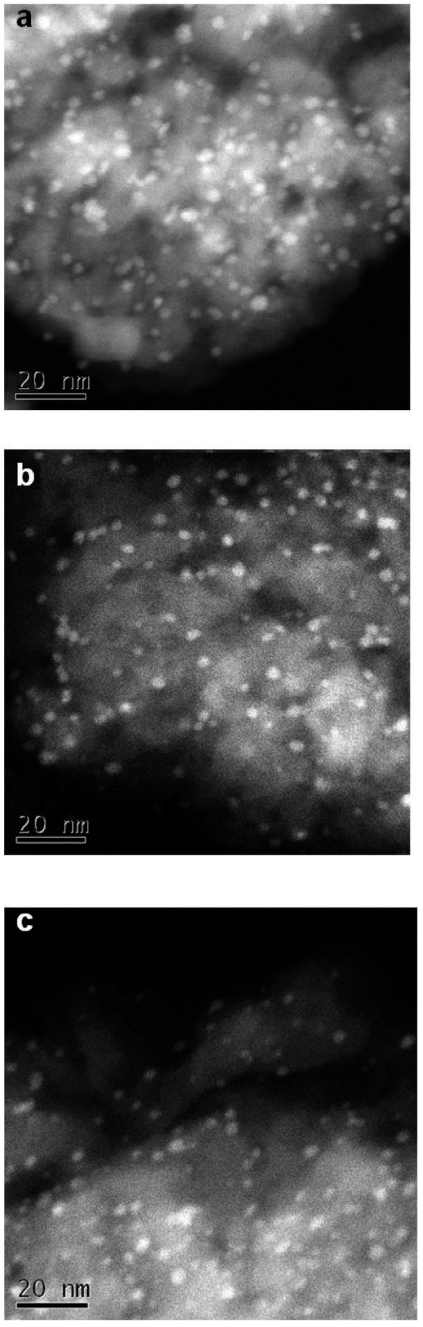

Figure 5. HAADF images of gold nanoparticles supported on (a) Y-TiO_2 (1-99)-N, (b) Y-TiO_2 (3-97)-N, (c) Y-TiO_2 (6-94)-N.

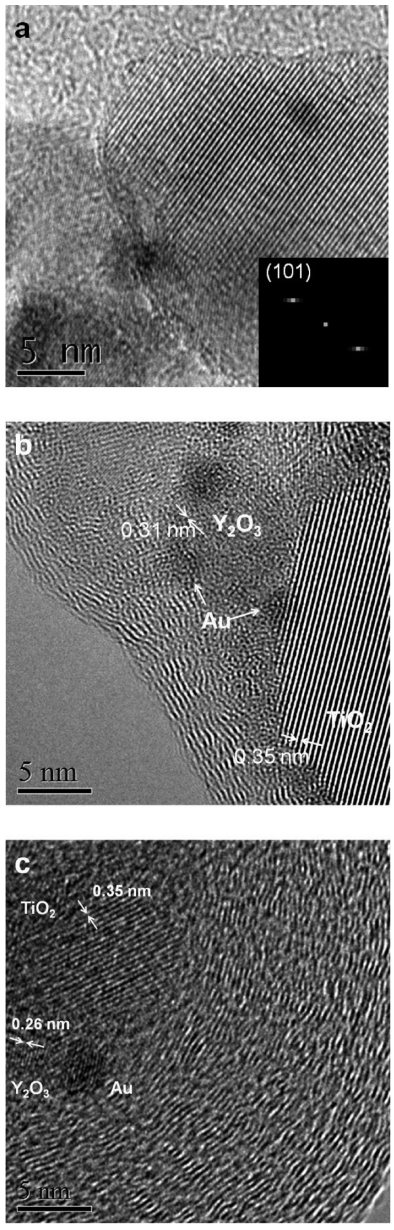

Figure 6. HRTEM images of (a) Au/Y-TiO_2(1-99)-N, (b) Au/Y-TiO_2(6-94)-N, (c) Au/Y-TiO_2(6-94)-Ac.

presence of gold in the metallic phase.[72,73] The intensity of the plasmon band is similar in all the samples and confirms the similar content of gold (~3%), similar particles size, and similar particle shape. The band gap energies (Eg) of the gold-containing catalysts are red-shifted in the same proportion (~0.3 nm) in comparison with the Y-TiO_2 samples.

3.3. CO Oxidation Activity and Temporal Stability. Figure 8 shows the conversion of CO as a function of the reaction temperature for the Au/Y-TiO_2 catalysts after activation under air at 300 °C. The catalytic activity of the Au/TiO_2 catalysts is also reported for comparison. The Au/TiO_2 sample is already active at 0 °C (CO conversion ≈46%), at room temperature the conversion of Au/TiO_2 is about 53%, whereas at this temperature, all the Au/Y-TiO_2 samples show a higher conversion than Au/TiO_2 (Figure 8). It is important to note that the CO conversion depends on the Y loading on the support. The highest conversions as a function of the reaction temperature were obtained with both Y-TiO_2 (1-99)-N and Y-TiO_2 (1-99)-Ac catalysts, that is, with a Y loading of about 0.6 wt % (Table 1). When the Y loading was increased (theoretical Y loadings of 3 and 6 wt %), the CO conversion decreased; however, it was always higher than the one obtained from Au/TiO_2 for room temperature and higher temperatures. As shown in Figure 8, when yttrium oxide is present on the surface of TiO_2 particles, mainly in the case of the 6 wt % Y loading, the CO conversion is lower than that of Au/TiO_2 at very low temperature (0 °C).

The catalytic results show that the creation of defects on the support surface by the incorporation of yttrium into the titania

dx.doi.org/10.1021/cs200332v |*ACS Catal.* 2012, 2, 1–11

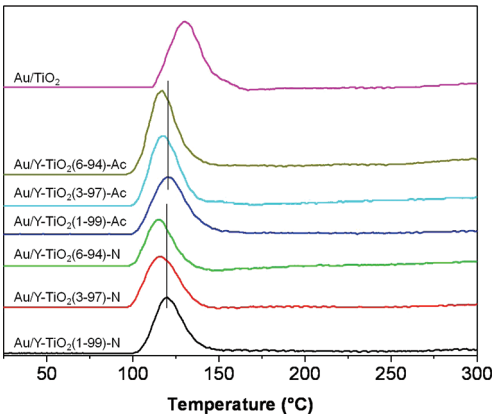

Figure 7. TPR profiles of the studied catalysts.

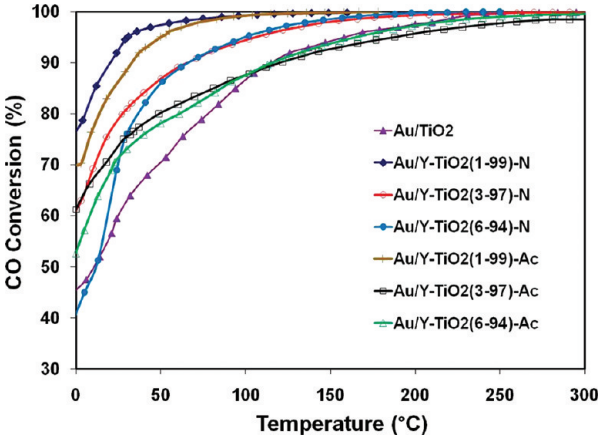

Figure 8. CO oxidation light-off curves of gold catalysts supported on TiO_2 (P25) and Y-TiO_2 samples.

lattice, accompanied by the creation of oxygen vacancies, as shown by PL and by HRTEM results, increases the catalytic activity in the CO oxidation reaction. It has been previously proposed that the incorporation of yttrium in the titania lattice favors the formation of oxygen vacancies.[50] When the catalyst is doped, vacancies on the surface of the support particles are created.[49,50,74] These vacancies generate crystalline defects that work as pinning centers for the gold particles.[18,75] The amount of dopant controls the number of surface oxygen vacancies created as well as the gold particle size, which directly affects the catalytic activity. For the Au/TiO_2 catalysts, theoretical calculations have demonstrated that the gold particles bind stronger to a defect-rich surface than to a defect-deficient surface of the titania particles and, that a significant charge transfer from the titania to the Au particles occurs.[32,33,35] In the case of Y-TiO_2 catalysts it is likely that the defect sites on TiO_2 helps to activate O_2 while Au nanoparticles in proximity to these defect sites activate CO, leading to better CO oxidation performance. It has been also proposed that oxygen vacancies on the support have an important role in activating O_2[76−78] because they can react with O_2 to form peroxide and superoxide species. In the presence of gold nanoparticles on the TiO_2 surface the superoxide species become highly reactive, and the activity of the supported gold catalysts for CO oxidation increases.[77]

Assuming that Y in Y-TiO_2 (1-99) catalysts was completely doping TiO_2 (substituting Ti atoms by Y atoms), the highest

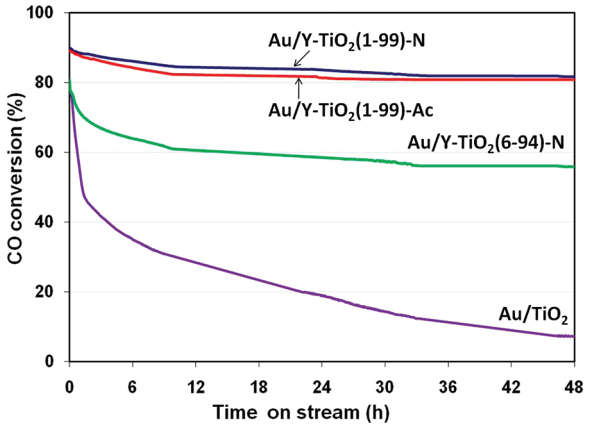

Figure 9. Evolution of the CO oxidation activity as a function of time on stream, at 15 °C, for the Au/TiO_2 and gold supported on Y-TiO_2 (1-99)-N, Y-TiO_2 (1-99)-Ac, and Y-TiO_2 (6-94)-N oxides.

catalytic activity observed for these catalysts could be explained by the surface defects created during the doping process. In the case of Y-TiO_2 (3-97) and Y-TiO_2 (6-94), yttrium could not substitute more Ti atoms so small Y_2O_3 crystals are formed on the surface of TiO_2. Some gold particles could have deposited on these Y_2O_3 crystals. As Y_2O_3 is a nonreducible oxide, the catalytic activity of Au/Y_2O_3 decreased when the Y loading increased in the support because the Y_2O_3 crystals on the surface increased; however, the CO conversion of Y-TiO_2 (3-97) and Y-TiO_2 (6-94) is higher at room temperature than that of Au/TiO_2 because in these mixed supports some of Y was doping TiO_2 which creates defects where gold particles could be also deposited, so the sum of the activities (Au supported on defect TiO_2 sites + Au supported on Y_2O_3 nanocrystals) produced catalysts with catalytic activity higher than that of Au/TiO_2 but lower than that of Au/Y-TiO_2(1-99) where most of Y was doping TiO_2.

To determine the stability of the Au/Y-TiO_2 catalysts, time-on-stream experiments were performed at 15 °C for 48 h. Figure 9 shows the results of Au/TiO_2, Au/Y-TiO_2 (1-99)-N, Au/Y-TiO_2 (1-99)-Ac, and Au-TiO_2 (6-94)-N catalysts activated in air at 300 °C. As can be observed in Figure 9, in addition to the increase of the activity because of the production of defects on the support, the Au/Y-TiO_2 catalysts exhibit a much better stability than the monometallic gold catalysts in the reaction of CO oxidation; while Au/TiO_2 deactivates continuously during the 48 h on stream, both Au/Y-TiO_2 (1-99)-N and Au/Y-TiO_2 (1-99)-Ac catalysts deactivate much less than Au/TiO_2. While Au/TiO_2 decreased its initial CO conversion from 79% to 8% after 48 h (loss of activity of 90%), the Au/Y-TiO_2 (1-99)-N changed its CO conversion from 88% to 82% (loss of activity of 7%); the behavior of the Au/Y-TiO_2 (1-99)-Ac was very similar to this last catalyst (loss of activity of 8%). In the case of catalyst Au-TiO_2 (6-94)-N, the loss of activity was about 28% after 48 h of time on stream. This catalyst was less stable than the catalysts doped with 1 wt % of Y, but it was more stable than the Au/TiO_2 catalyst. It is important to note that while the Au/TiO_2 catalyst deactivates during all the time of the test, the Au/Y-TiO_2 catalysts become stable after about 30 h on stream (Figure 9). The initial decrease of activity within the first hours of reaction observed in Figure 9 could be explained by the formations of surface carbonates.[18,24] In a previous study using TiO_2 catalysts containing In, we have shown that the Au/In-TiO_2 catalyst also

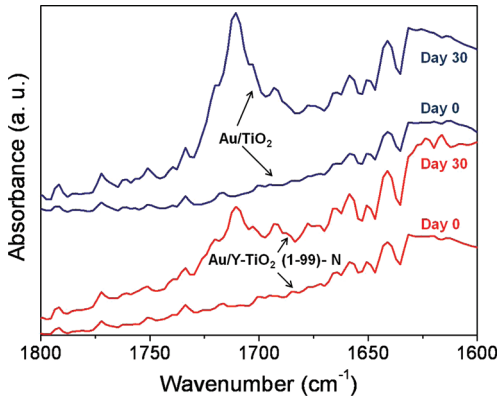

Figure 10. FTIR spectra of the Au/TiO_2 and $Au/Y\text{-}TiO_2$(1-99)-N catalysts just after activation (day 0) and aged in reaction conditions for 30 days.

presented an enhanced stability compared to gold catalysts supported on TiO_2 synthesized by the sol−gel method; however, after 46 h on stream, $Au/In\text{-}TiO_2$ lost 37% of its activity, and it became stable after about 40 h on stream; Au/TiO_2 sol−gel catalysts, as in the case of Au/TiO_2 (P25), continued to deactivate throughout the test (46 h) so the catalysts doped with yttrium seem to be more stable than the catalysts doped with indium.

To understand the origin of the differences in stability of doped and undoped catalysts, the $Au/Y\text{-}TiO_2$ (1-99)-N and the Au/TiO_2 catalysts were exposed at reaction conditions (flow of CO + O_2 in N_2 at 15 °C) for 30 days. Both catalysts were analyzed just after activation (day 0) and after 30 days under reaction by FTIR and TEM. The FTIR experiments were carried out to know if the differences in the deactivation of both catalysts were related to the adsorption of carbonates. The absorption spectrum of the fresh catalyst (Figure 10) presented some low-intensity bands in the carboxylate region, 1400−1800 cm^{-1}, that are characteristic of adsorbed carbonates.[79,80] When the catalysts were aged, the intensity of some bands increased, mainly those appearing at 1710 cm^{-1} (Figure 10), which corresponds to an asymmetric stretching of a side-on bend of CO_2-carboxylate species adsorbed on Ti^{3+} sites in close contact with the gold particles.[81] These species are known to be intermediate phases during the formation of carbonates and bicarbonates on a catalyst surface.[82] The intensity of the band related with carbonate species was very different in the Au/TiO_2 catalyst compared with that in the $Au/Y\text{-}TiO_2$ (1-99)-N one, being much more intense in the catalyst supported on the bare TiO_2. The presence of these carbonates in the gold catalysts, however, has been related not only to unreactive species that block the active sites[19,83−85] but also to intermediate products that might represent a key step in the catalytic oxidation of carbon monoxide.[86−88] Because during the FTIR analysis the catalysts were not under the reaction conditions for the oxidation of CO, the carbonate species observed on the catalysts during their analysis must be related to species that blocked the active sites.

TEM results showed that while the average gold particle size practically did not change for the $Au/Y\text{-}TiO_2$ (1-99)-N catalyst (3.0 nm for day 0 vs 3.1 nm for day 30), in the case of Au/TiO_2 catalysts, the average gold particle size increased from 3.1 to 3.6 nm after 30 days under reaction conditions. Therefore, the doping of the catalysts has a double effect: it prevents carbonates from forming and the gold particle from sintering during the reaction.

The higher stability of $Au/Y\text{-}TiO_2$ catalysts can be explained by the defects created by doping the support, which could have trapped the initial gold atoms that worked as seeds for the formation of gold particles; this interaction was more favorable than the interaction between the gold atoms and a local environment rich in oxygen. The affinity of the gold atoms with the defects on the titania surface produced a strong interaction between them, which stabilized the gold particles. Platas et al. have shown that on a doped-dehydrated surface, there is a larger difference in the binding energy of the gold atom at the vacancy or at nearby sites (−0.81 to −0.64 eV) with respect to other sites at the surface (−0.49 to −0.37 eV).[50] This means that the vacancies will play a double role. First, they favor the dispersion of the metal NPs over the surface as the number of vacancies increases with the yttrium loading and, second, they will act as nucleation sites that will strongly anchor those metal nanoclusters, reducing the sintering processes.

4. CONCLUSIONS

It was shown that the BET surface area of $Y\text{-}TiO_2$ prepared by the sol−gel method increased with the Y content because the increase of the Y content on the support prevented the growth of the crystallite size of the anatase crystals. Moreover, the incorporation of yttrium restricts the transformation of the TiO_2 anatase phase to the rutile TiO_2 phase. Because of the big difference in the atomic radius of Y^{3+} and Ti^{4+}, the substitution of Ti^{4+} by Y^{3+} cations in the titania framework was limited to low Y loadings. High contents of Y produced the segregation of yttrium as Y_2O_3 on the surface of TiO_2. The incorporation of yttrium in TiO_2 lattice favored the formation of oxygen vacancies, which are the preferred adsorption sites for Au nanoparticles, acting as nucleation centers for Au atoms.

Using the urea deposition-precipitation method, gold particles with average particle size of 3 nm were deposited on $Y\text{-}TiO_2$ and TiO_2 (P25) supports. $Au/Y\text{-}TiO_2$ catalysts showed higher activity and stability at room temperature than Au/TiO_2. The highest activities and stabilities as a function of time on stream were observed for $Au/Y\text{-}TiO_2$ (1-99), in which it is proposed that all Y was doping TiO_2. This behavior is related to the strong anchoring of the gold particles on the structural defects of the support caused by the doping of the anatase with yttrium, which naturally gives rise to structures with oxygen vacancies. The gold particles bind stronger to a defect-rich surface than to a defect-deficient surface of the titania particles and a significant charge transfer from the titania to the Au particles occurs. HRTEM results show that at high content of Y, Y_2O_3 is segregated on the surface of TiO_2. As Y_2O_3 is a not reducible oxide, when it was on the TiO_2 surface, the catalytic activity of the $Au/Y\text{-}TiO_2$ catalyst decreased; however, it was always higher than that obtained from Au/TiO_2 at room temperature and higher temperatures. The higher stability of the $Au/Y\text{-}TiO_2$ catalysts compared with that of the Au/TiO_2 catalyst is due to lower carbonate formation and to lower gold particle sintering during the reaction.

AUTHOR INFORMATION

Corresponding Author

*E-mail: rodolfo.zanella@ccadet.unam.mx. Phone: +52(55)56228635. Fax +52 (55) 55500654.

Funding Sources

We are grateful for the financial support received via PAPIIT IN108310 and CONACYT 130407 projects and the Nanoscience and Nanotechnology CONACYT network.

■ ACKNOWLEDGMENT

We thank Viridiana Maturano and Elsi Mejía for PL characterization of the samples and Beatriz A. Rivera-Escoto for the Raman and TEM characterization of the supports. We also thank Mariana Hinojosa-Reyes for valuable technical assistance in the experimental work.

■ REFERENCES

(1) Bond, G. C. *Catal. Today* **2002**, *72*, 5.
(2) Moreau, F.; Bond, G. C. *Catal. Today* **2007**, *122*, 215.
(3) Bond, G. C.; Louis, C.; Thompson, D. T. *Catalysis by Gold*, 1st ed.; Imperial College Press: London, 2006; Vol. 6.
(4) Roldan-Cuenya, B. *Thin Solid Films* **2010**, *518*, 3127.
(5) Haruta, M.; Kobayashi, T.; Sano, H.; Yamada, N. *Chem. Lett.* **1987**, *2*, 405.
(6) Gong, J.; Mullins, C. B. *Acc. Chem. Res.* **2009**, *42*, 1063.
(7) Bond, G. C.; Thompson, D. T. *Catal. Rev.-Sci. Eng.* **1999**, *41*, 319.
(8) Bokhimi, X.; Zanella, R.; Morales, A. *J. Phys Chem. C* **2007**, *111*, 15210.
(9) Haruta, M. *Chem. Rec.* **2003**, *3*, 75.
(10) Zanella, R.; Giorgio, S.; Shin, C. H.; Henry, C. R.; Louis, C. *J. Catal.* **2004**, *222*, 357.
(11) Laoufi, I.; Saint-Lager, M. C.; Lazzari, R.; Jupille, J.; Robach, O.; Cabailh, S. G. G.; Dolle, P.; Cruguel, H.; Bailly, A. *J. Phys. Chem. C* **2011**, *115*, 4673–4679.
(12) Rodríguez-González, V.; Zanella, R.; del-Angel, G.; Gómez, R. *J. Mol. Catal. A* **2008**, *281*, 93.
(13) Haruta, M. *Catal. Today* **1997**, *36*, 153.
(14) Grunwaldt, J.-D.; Baiker, A. *J. Catal.* **1999**, *181*, 223.
(15) Zanella, R.; Giorgio, S.; Henry, C. R.; Louis, C. *J. Phys. Chem. B* **2002**, *106*, 7634.
(16) Zanella, R.; Louis, C. *Catal. Today* **2005**, *107*−*108*, 768.
(17) Bokhimi, X.; Zanella, R.; Morales, A. *J. Phys. Chem. C* **2008**, *112*, 12463.
(18) Bokhimi, X.; Zanella, R.; Morales, A.; Maturano, V.; Ángeles-Chávez, C. *J. Phys. Chem. C* **2011**, *115*, 5856.
(19) Konova, P.; Naydenov, A.; Venkov, C.; Mehandjiev, D.; Andreeva, D.; Tabakova, T. *J. Mol. Catal. A* **2004**, *213*, 235.
(20) Andreeva, D. *Gold Bull.* **2002**, *35*, 82.
(21) Bokhimi, X.; Zanella, R.; Morales, A. *Open Inorg. Chem. J.* **2009**, *3*, 69.
(22) Raphulu, M. C.; McPherson, J.; van-der-Lingen, E.; Anderson, J. A.; Scurrell, M. S. *Gold Bull.* **2010**, *43*, 334.
(23) Hao, Y.; Milhaylov, M.; Ivanova, E.; Hadjivanov, K.; Knözinger, H.; Gates, B. C. *J. Catal.* **2009**, *261*, 137.
(24) Bokhimi, X.; Zanella, R.; Angeles, C. *J. Phys. Chem. C* **2010**, *114*, 14101.
(25) Kolmakov, A.; Goodman, D. W. *Catal. Lett.* **2000**, *70*, 93.
(26) Kielbassa, S.; Kinne, M.; Behm, R. J. *J. Phys. Chem. B* **2004**, *108*, 19184.
(27) http://www.premchemltd.com/runtime/uploads/Files/Premier_Chemicals_NanAucat_Gold_Catalyst_Brochure.pdf.
(28) Diebold, U.; Anderson, F. F.; Ng, K. O.; Vanderbilt, D. *Phys. Rev. Lett.* **1996**, *77*, 1322.
(29) Li, M.; Hebensteit, W.; Diebold, U.; Tyrayshkin, M.; Bowman, M. K.; Dunham, G. G.; Henderson, M. A. *J. Phys. Chem. B* **2000**, *104*, 4944.
(30) Maciejewski, M.; Fabrizioli, P.; Grunwaldt, J. D.; Becker, O. S.; Baiker, A. *Phys. Chem. Chem. Phys.* **2001**, *3*, 3846.
(31) Lopez, N.; Norskov, J. K.; Janssens, T. V. W.; Carlsson, A.; Puig-Molina, A.; Clausen, B. S.; Grunwaldt, J.-D. *J. Catal.* **2004**, *225*, 86.
(32) Lopez, N.; Janssens, T. V. W.; Clausen, B. S.; Xu, Y.; Mavrikakis, M.; Bligaard, T.; Norskov, J. K. *J. Catal.* **2004**, *223*, 232.
(33) Rodríguez, J. A.; Liu, G.; Jirsak, T.; Hrbek, J.; Chang, Z. P.; Dvorak, J.; Marti, A. *J. Am. Chem. Soc.* **2002**, *124*, 5242.
(34) Liu, L. M.; McAllister, B.; Ye, H. Q.; Hu, P. *J. Am. Chem. Soc.* **2006**, *128*, 4017.
(35) Laursen, S.; Linic, S. *Phys. Rev. Lett.* **2006**, *97*, 026101.
(36) Liu, Z. P.; Jenkins, S. J.; King, D. A. *Phys. Rev. Lett.* **2004**, *93*, 156102.
(37) Wang, C.-M.; Fan, K.-N.; Liu, Z.-P. *J. Phys. Chem. C* **2007**, *111*, 13539.
(38) Hou, K.-J.; Meng, M.; Zou, Z.-Q.; Lu, Q. *Chin. J. Inorg. Chem.* **2007**, *23*, 1538.
(39) Ma, Z.; Overbury, S. H.; Dai, S. *J. Mol. Catal. A* **2007**, *273*, 186.
(40) Debeila, M. A.; Wells, R. P. K; Anderson, J. A. *J. Catal.* **2006**, *239*, 162.
(41) Moreau, F.; Bond, G. C. *Top. Catal.* **2007**, *44*, 95.
(42) Grisel, R. J. H.; Kooyman, P. J.; Nieuwenhuys, B. E. *J. Catal.* **2000**, *191*, 430.
(43) Grisel, R. J. H.; Nieuwenhuys, B. E. *Catal. Today* **2001**, *64*, 69.
(44) Tai, Y.; Murakami, J.; Tajiri, K.; Ohashi, F.; Daté, M.; Tsubota, S. *Appl. Catal., A* **2004**, *268*, 183.
(45) Venezia, A. M.; Liotta, F. L.; Pantaleo, G.; Beck, A.; Horvath, A.; Geszti, O.; Kocsonya, A.; Guczi, L. *Appl. Catal., A* **2006**, *310*, 114.
(46) Yan, W.; Mahurin, S. M.; Pan, Z.; Overbury, S. H.; Dai, S. *J. Am. Chem. Soc.* **2005**, *127*, 10480.
(47) Moreau, F.; Bond, G. C. *Catal. Today* **2006**, *114*, 362.
(48) Min, B. K.; Wallace, W. T.; Goodman, D. W. *J. Phys Chem. B* **2004**, *108*, 14609.
(49) Rodríguez-González, V.; Zanella, R.; Calzada, L. A.; Gómez, R. *J. Phys Chem. C* **2009**, *113*, 8911.
(50) Plata, J. J.; Márquez, A. M.; Fdez-Sanz, J.; Sáncehz-Avellaneda, R.; Romero-Sarria, F.; Domínguez, M. I.; Centeno, M. A.; Odriozola, J. A. *Top. Catal.* **2011**, *54*, 219.
(51) Zanella, R.; Delannoy, L.; Louis, C. *Appl. Catal., A* **2005**, *291*, 62.
(52) Kumar, K. N. P.; Keizer, K.; Burggraaf, A. J.; Okubo, T.; Nagamoto, H.; Morooka, S. *Nature* **1992**, *358*, 48.
(53) Ma, W.; Lu, Z.; Zhang, M. *Appl. Phys. A: Mater. Sci. Process.* **1998**, *66*, 621.
(54) Narayan, H.; Alemu, H.; Macheli, L.; Thakurdesai, M.; Rao, T. K. G. *Nanotechnology* **2009**, *20*, 255601.
(55) Schweitzer, G. K.; Pesterfield, L. L. *The Aqueous Chemistry of the Elements*; Oxford University Press, New York, 2010.
(56) Jung, K. Y.; Park, S. B.; Anpo, M. *J. Photochem. Photobiol. A* **2005**, *170*, 247.
(57) Anpo, M.; Aikawa, N.; Kubokawa, Y.; Che, M.; Louis, C.; Giamello, E. *J. Phys. Chem.* **1985**, *89*, 5017.
(58) Bieber, H.; Gillot, P.; Gallart, M.; Keller, N.; Keller, V.; Bégin-Colin, S.; Pighini, C.; Millot, N. *Catal. Today* **2007**, *122*, 101.
(59) Memesa, M.; Lenz, S.; Emmerling, S. G. J.; Nett, S.; Perlich, J.; Müller-Buschbaum, P.; Gutmann, J. S. *Colloid Polym. Sci.* **2011**, *289*, 943.
(60) Zhang, W. F.; Zhang, M. S.; Yin, A.; Chen, Q. *Appl. Phys. B: Laser Opt.* **2000**, *70*, 261.
(61) Sun, Z. C.; Wolkenhauer, M.; Bumbu, G. G.; Knoll, W.; Gutmann, J. S. *Chem. Phys. Chem.* **2006**, *7*, 370.
(62) Nakamura, R.; Okamura, T.; Ohashi, N.; Imanishi, A.; Nakato, Y. *J. Am. Chem. Soc.* **2005**, *127*, 12975.
(63) Tang, H.; Berger, H.; Schmid, P. E.; Levy, F.; Buri, G. *Solid State Commun.* **1993**, *87*, 847.
(64) Serpone, N.; Lawless, D.; Khairutdinov, R. *J. Phys. Chem.* **1995**, *99*, 16646.
(65) Forss, L.; Schubnell, M. *Appl. Phys. B: Laser Opt.* **1993**, *56*, 363.
(66) Serpone, N. *J. Phys Chem. B* **2006**, *110*, 24287.
(67) Baiju, K. V.; Zachariah, A.; Shukla, S.; Biju, S.; Reddy, M. L. P.; Warrier, K. G. K. *Catal. Lett.* **2009**, *130*, 130.
(68) Sandoval, A.; Gómez-Cortés, A.; Zanella, R.; Díaz, G.; Saniger, J. M. *J. Mol. Catal. A* **2007**, *278*, 200.
(69) Andreeva, D.; Tabakova, T.; Ilieva, L.; Naydenov, A.; Mehanjiev, D.; Abrashev, M. V. *Appl. Catal., A* **2001**, *209*, 291.
(70) Idakiev, V.; Ilieva, L.; Andreeva, D.; Blin, J. L.; Gigot, L.; Su, B. L. *Appl. Catal., A* **2003**, *243*, 25.

(71) Trovarelli, T. A. *Catal. Rev.-Sci. Eng.* **1996**, *38*, 439.
(72) Reyes-Esqueda, J. A.; Buatista-Salvador, A.; Zanella, R. *J. Nanosci. Nanotechnol.* **2008**, *8*, 3843.
(73) Morales-Saavedra, O. G.; Zanella, R. *Mater. Chem. Phys.* **2010**, *124*, 816.
(74) Andreeva, D.; Ivanov, I.; Ilieva, L.; Abrashev, M. V.; Zanella, R.; Sobczak, J. W.; Lisowski, W.; Kantcheva, M.; Avdeev, G.; Petrov, K. *Appl. Catal., A* **2009**, *357*, 159.
(75) Chen, M. S.; Goodman, D. W. *Top. Catal.* **2007**, *44*, 41.
(76) Bond, G.; Thompson, D. *Gold Bull.* **2009**, *42*, 247.
(77) Carrettin, S.; Hao, Y.; Aguilar-Guerrero, V.; Gates, B. C.; Trasobares, S.; Calvino, J. J.; Corma, A. *Chem.—Eur. J.* **2007**, *13*, 7771.
(78) Liu, H.; Kozlov, A. I.; Kozlova, A. P.; Shido, T.; Asakura, K.; Iwasawa, Y. *J. Catal.* **1999**, *185*, 252.
(79) Iojoiu, E.; Gélin, P.; Praliaud, H.; Primet, M. *Appl. Catal., A* **2004**, *263*, 39.
(80) Davydov, A. A. *Infrared Spectroscopy of Adsorbed Species on the Surface of Transition Metal Oxides*; Rochester, C.H., Ed.; John Wiley & Sons: New York, 1984.
(81) Boccuzzi, F.; Chiorino, A.; Manzoli, M.; Andreeva, D.; Tabakova, T. *J. Catal.* **1999**, *188*, 176.
(82) Ramis, G.; Busca, G.; Lorenzelli, V. *Mater. Chem. Phys.* **1991**, *29*, 425.
(83) Haruta, M. *Cattech* **2002**, *6*, 102.
(84) Schubert, M. M.; Plzak, V.; Garche, J.; Behm, R. J. *Catal. Lett.* **2001**, *76*, 143.
(85) Haruta, M.; Daté, M. *Appl. Catal., A* **2001**, *222*, 427.
(86) Socaciu, L. D.; Hagen, J.; Brenhardt, T. M.; Wöste, L.; Heiz, U.; Bligaard, T.; Landman, U. *J. Am. Chem. Soc.* **2003**, *125*, 10437.
(87) Liu, Z.-P.; Hu, P.; Alavi, A. *J. Am. Chem. Soc.* **2002**, *124*, 14770.
(88) Daniells, S. T.; Overweg, A. R.; Makkee, M.; Moulijn, J. A. *J. Catal.* **2005**, *230*, 52.